# A QM/MM study of Kemptide phosphorylation catalyzed by Protein Kinase A. The role of Asp166 as a general acid/base catalyst.

Ayax Pérez-Gallegos, Mireia Garcia-Viloca, Àngels González-Lafont* and José M. Lluch

*Institut de Biotecnologia i de Biomedicina and Departament de Química, Universitat Autònoma de Barcelona, 08193 Bellaterra (Barcelona), Spain. E-mail: Angels.Gonzalez@uab.cat*

**Abstract:** In this work a theoretical study of the γ-phosphoryl group transfer from ATP to Ser17 of the synthetic substrate Kemptide (LRRASLG) in Protein Kinase A (PKA) has been carried out with a solvated model of the PKA-$Mg_2$ATP-Kemptide system based on the 1CDK X-ray crystallographic structure. We have used high levels (B3LYP/MM and MP2/MM) of theory to determine the overall reaction paths of the so-called concerted loose mechanism trying to clarify some aspects of that mechanism still under debate. Our calculations demonstrate for the first time in a complete model of the ternary system the viability of the final step of the catalytic mechanism in which the protonation of the phosphokemptide product by Asp166 takes place. Asp166 is a base catalyst that abstracts the HγSer17 of Kemptide thus facilitating the phosphoryl transfer, but Asp166 also acts as an acid catalyst by donating the proton just accepted from Ser17 to the O2γATP atom of the phosphoryl group.

**Introduction**

Protein kinases are key-enzymes in cellular signaling pathways because they catalyze the post-translational modification of protein residues by means of phosphorylation. Phosphorylation is the central regulation mechanism of mammalian protein functions in living cells, in this way regulating basic cell processes.[1] For this reason, protein kinases have become the most relevant drug targets for cancer therapy in the last fifteen years and growing interest in targeting kinases has also now been extended to the area of inflammatory diseases.[2] In turn, most protein kinases are also phosphoproteins.[3]

Among the superfamily of protein kinases, cyclic adenosine monophosphate (cAMP)–dependent protein kinase A (PKA) (a serine/threonine protein kinase) was the first to be analyzed[4] and its crystallographic structure the first to be solved.[5, 6] The PKA catalytically active subunit (PKAc) is also the best characterized among protein kinases and, as its core is highly conserved, PKAc has been used as a model enzyme for the rest of family members.[7-9] PKAc recognizes and phosphorylates the amino acid sequence R-R-X-S/T-Z which is present in hundreds of cellular substrates (S/T is the phosphorylation (P) site, the P-2 and P-3 positions are occupied by two arginines (R), X stands for any residue and Z is a hydrophobic residue).[10] Following this sequence pattern of residues, a synthetic substrate called Kemptide[11] was designed (LRRASLG) in 1977 showing kinetic constants comparable to native protein substrates.[12-14] Very recently, Kemptide substrate has been used again to prove by Molecular Dynamics simulations the cooperativity of ATP and Kemptide binding to PKAc,[15] and also in single molecule experiments to prove the conformational variability of the PKAc-ATP$Mg_2$-Kemptide complex.[16]

Even though PKAc is one of the best understood kinases, there are still many old and new questions without a complete satisfying answer that have recently been analyzed and debated in the literature extending the discussion to the functioning of other kinases.[17-21] Some of those questions are the following: 1) How does the transition state character of the catalytic mechanism depend on the structure of the enzyme and on the substrate?[18-20] Here a discussion on the proper way to characterize and denominate the phosphorylation catalytic mechanisms (associative versus dissociative, or concerted versus dissociative/associative, and concerted tight versus concerted loose) has been put forward.[19] With regard to this point, from here on in this paper we use the IUPAC nomenclature. That is, the dissociative and associative mechanisms (when using the definition given by Warshel and coworkers for a phosphate monoester hydrolysis in aqueous solution)[22, 23] will be both called here concerted mechanisms ($A_ND_N$). The difference between them being the transition state nature which can be described as loose or tight.[19, 24] That is, the concerted loose transition state implies an

almost complete break of the bond between the ADP and the metaphosphate leaving group while the new bond with the nucleophile serine residue hardly begins to be formed. Conversely, in the concerted tight transition state the bond formation with the substrate serine residue starts when the ADP and the γ-phosphate leaving group are still quite closely connected. The nucleophile and leaving group may be bonded to phosphorus to differing extents at the transition states. Other questions are: 2) What is the origin of the phosphoryl-transfer transition state stabilization?[25] 3) Which is the exact role of metal ions and some particular residues in the catalytic mechanism?[18, 19, 21, 26] 4) Which are the conformational fluctuations of PKAc linked with enzymatic turnover? 5) Which are the key conformational states along the catalytic cycle?[27, 28] 6) What are the driving forces for the release of the phosphorylated product and ADP?[29]

All these questions have motivated an intense revival of the interest for the catalytic mechanism of PKA and other kinases.[30-38] In this respect, a number of crystallographic structures of the ternary nucleotide-substrate/inhibitor-bound PKAc complexes have been released. Those structures are experimental snapshots of the catalytic cycle and the comparison of those structures with X-ray binary (nucleotide/substrate-bound PKAc) complexes and apo crystals have revealed the major conformational states (open, intermediate and closed) of PKAc complexes along the catalytic pathway.[28, 39] That structural information has been recently complemented by dynamic analyses based on NMR experiments, and molecular dynamics simulations.[27, 40, 41] These studies provided very interesting insights into the dynamic fluctuations of the protein needed for turnover and for the regulation mechanisms in which kinases behave as signal switches.

However, several crystallographic structures of PKAc complexes recently deposited in the PDB have also been used to elucidate molecular details of the chemical step of the phosphorylation process as well as to provide more information on the role of magnesium ions, along with new aspects of the products release step.[18, 19, 42, 43] In particular, Taylor and coworkers have recently launched two new X-ray structures of ternary PKAc-$Mg_2$AMP-PNP-SP20 (SP20 is a 20-residue substrate) complexes showing partial and total phosphoryl transfer, respectively.[18] Those structures seem to indicate according to the authors that one of the magnesium ions (Mg1) could probably be expelled first from the active site after phosphoryl transfer, and preceding ADP release, while Mg2 would remain bound with ADP. As for the orientation of the serine substrate residue, in both structures $Ser21_{SP20}$ is flipped away from Asp166. In contrast, in the 1L3R transition state (TS) mimic structure[44] with a concerted loose character and assisted by the Asp166 residue as a catalytic base, the OH group of the serine residue is facing Asp166 at hydrogen-bond distance of its carboxylate group. In a nearly

concomitant paper, Kovalevsky and coworkers[19] have also determined the structure of another ternary pseudo-Michaelis complex, PKAc−$Mg_2$AMP-PCP−SP20, as well as the structure of a ternary PKAc−$Mg_2$ADP−pSP20 complex with both products, the phosphorylated substrate (pSP20) and ADP, trapped in the active site. The analysis of those structures reveals an important conformational change of the $Ser21_{SP20}$ side chain that rotates from its initial orientation, with a potential hydrogen bond between the serine OH group and one oxygen atom of the γ-$PO_3^{2-}$ group, to that with the serine OH group facing Asp166 at the transition state. According to the authors that $Ser21_{SP20}$ side chain movement could be the driving force of the chemical step and might prepare the phosphorylated product for release from the enzyme because at the product complex structure the side chain of $Ser21_{SP20}$ has rotated now towards the solvent. In any case, the authors clearly indicate that those conclusions about the chemical mechanism might depend on the substrate, and they claim that theoretical calculations could confirm that those crystallographic structures along with the earlier TS mimic structure (1L3R),[44] do really represent sequential conformations on the reaction pathway of the phosphoryl transfer with the requirement that a proper location of the hydrogen atoms before and after the chemical step is used in the computational models.

In fact, a number of theoretical studies have already been published on the catalytic mechanism of PKAc. Several groups have investigated the phosphoryl transfer and phosphorylation mechanisms catalyzed by PKAc using semiempirical[45, 46] or ab initio and/or DFT quantum mechanical (QM) methods with cluster models,[30, 31] or carrying out semiempirical or DFT quantum mechanical/molecular mechanics (QM/MM) calculations as well as molecular dynamics (MD) simulations using more complete models of the solvated ternary PKAc complex.[31-36, 38, 47] In some of those studies the 1ATP X-ray structure[48] corresponding to a ground-state analogue was used as the initial coordinates[30, 32, 34] or the TS mimic structure 1L3R.[32, 33] Díaz and Field[31] used the 1CDK X-ray structure[49] and in our previous work we compared the phoshoryl transfer mechanism with 1ATP and 1CDK X-ray structures.[36] The substrates chosen in those studies are $HOCH_2CH_3$ (substrate model),[30] Kemptide,[35, 36] a 20-residue peptide substrate with the sequence TTYADFIASGRTGRRNSIHD (obtained from the PKI inhibitor by mutating Ala by Ser)[31] and the SP20 molecule.[32-34] Most of those theoretical studies conclude that the most favorable mechanism is the concerted loose pathway in which the nucleophilicity of the Ser residue is assisted by a late proton transfer to residue Asp166 that participates as a catalytic base. This catalytically active role of Asp166 is in agreement with previous crystallographic data and kinetic measurements.[10, 50] Kinetic experiments[51] on the Asp149Ala and Asp149Asn mutants of protein kinase PhK (Asp149 is the analogue of Asp166 in PKA) had shown a very important decrease of $k_{cat}$ in accordance with the null or reduced

capability of Ala and Asn, respectively, to behave as basic residues or even for positioning the serine nucleophile in the case of the Ala residue. The calculated potential energy barriers for the phosphoryl transfer in the mentioned cluster models go from 11.0 to 17.2 kcal/mol and in the enzyme models those values are in the range 11.6 to 18.3 kcal/mol. Weare and coworkers[34] report a 15 kcal/mol free energy barrier. Those energy barriers compare reasonably or quite well with the phosphoryl transfer rate constants of 500-154 $s^{-1}$,[14, 52, 53] measured for the burst phase of the reactions with different substrates, as the experimental phenomenological free energy barrier would be 14-15 kcal/mol according to conventional transition state theory.

On the other hand, a mechanistic aspect that clearly differentiates the energy profiles of the theoretical studies mentioned above is related with the product state of the phosphoryl transfer mechanism. In some studies the energy profile for the concerted loose pathway turns out to be endoergic (potential energy values in the range 10.1 to 16.7 kcal/mol have been reported)[31, 32, 36] whereas in others it is exoergic with a reaction potential energy of 9 kcal/mol[30] or exoergonic with a reaction free energy of 3 kcal/mol.[34] Moreover, only in the study by Díaz and Field[31] the reaction pathway corresponding to the proton transfer from Asp166 to one of the oxygen atoms of phosphorylated serine is analyzed. That reaction pathway connects the product structure of the phosphoryl transfer step (in which the proton of the serine residue has been completely transferred to the Asp166 residue) with a structure of the product complex with a protonated phosphoryl group and an unprotonated Asp166 residue. According to Díaz and Field[31] this last structure could facilitate the release of the phosphorylated product (with one negative net charge) because of the electrostatic repulsion with the negatively charged carboxylate group of Asp166. In fact, this hypothesis is based on the mutagenesis experiments carried out by Johnson and coworkers[51] on the Asp149Asn mutant of PhK. Those kinetic studies showed that this mutation greatly reduces the rate constant of the phosphorylation process (by a factor of around 2.2 x $10^3$) but also of the product departure (a fall of 4.5 x$10^3$) due to the impossibility of Asn to ionize according to the authors. In this way, Asp166 would in fact participate in the mechanism as an acid/base catalyst promoting the proton shuttle from the serine residue of the peptide substrate to the phosphoryl group of the phosphorylated peptide product. In contrast, Valiev et al.[30] stated that the protonation of the phosphoryl group at the product structure is unlikely because of its interactions with $Mg^{2+}$ ions.

Taking into account that the mechanism can depend on the substrate and on the crystal structure, the aim of the present paper is to analyze the complete phosphoryl transfer concerted loose mechanism catalyzed by PKAc using the 1CDK X-ray structure and Kemptide as

substrate. We will use the QM/MM approach at the DFT/MM level to locate the most relevant stationary points on the potential energy surface of the phosphoryl transfer mechanism by using flexible reaction coordinates. In our previous work only a semiempirical method to describe the QM part could be used (in particular the AM1/d-PhoT/MM hybrid scheme was employed) for the optimization of stationary points, and DFT electronic-structure calculations were used just for single point energy corrections.[36] Moreover, as indicated above, in our previous study the proton transfer from Asp166 to the phosphorylated peptide product was not analyzed. Here, special attention will be devoted to the specific role of Lys168 and Asp166 residues in the catalytic mechanism, as well as to the protonation state of the product complex after phosphoryl transfer and its relevance in the reaction energetics and in the phosphorylated peptide product release.

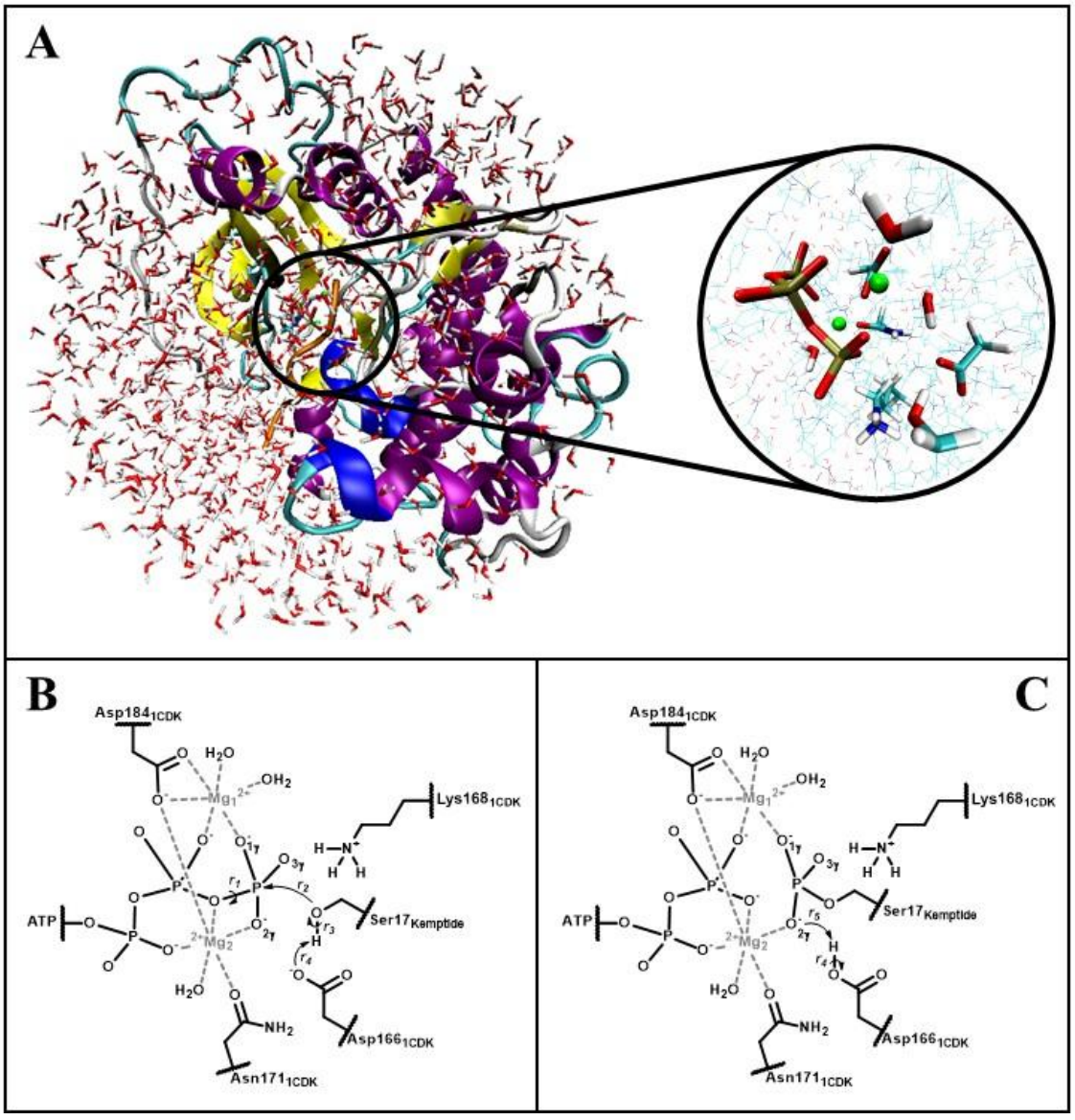

**Figure 1.** A) Structure of the PKA–$Mg_2$ATP–Kemptide complex solvated with a 25 Å-radius sphere of water molecules. The black circle highlights the position of the active site. In the inset an enlarged view of the active site is shown in atomistic rendering with the QM atoms represented in licorice style. Scheme of the concerted loose catalytic mechanism: B) Phosphoryl transfer step; C) Proton transfer step

**Models and Methods**

In a preceding work[38] on the associative mechanism (now called concerted tight) of the phosphoryl transfer catalyzed by the cAMP-dependent protein kinase A (PKA, whose catalytic subunit, PKAc, was initially represented by PDB code 1CDK X-ray structure,[49] so displaying a closed active conformation and having the residue Thr197 modified into a phospho-threonine), different structures generated during previous MD simulations[35] were considered as appropriate starting points to model the ternary Michaelis complex of PKA with ATP-$Mg_2$ and the synthetic heptapeptide Kemptide as substrate (Figure 1A). The same structures (named eq21, eq55, eq91, and M1)[35] have also been chosen here to simulate the concerted loose mechanism because the reactive $Ser17_{Kemptide}$, the γ-phosphoryl group of ATP, and the $Asp166_{PKA}$ within them, were close enough one another to allow the two mechanisms, neither favoring nor excluding any of them.

For the QM/MM calculations we have fractioned the system and we have defined the QM/MM partition following the same procedure we used in our previous study.[38] First, all non-ternary complex residues (basically, solvation – or TIP3 – water molecules) being more than 25 Å away from the geometric center of $O_\gamma$Ser17, $O3_\gamma$ATP, and $O_\delta$2Asp166 were deleted. Then, all residues and water molecules within 20 Å of such point were included in the optimization process as the active – or allowed to move freely – region, while the remainder were kept fixed in their positions along the subsequent optimizations and simulations (for the 1CDK-based models the number of active atoms in eq21, eq55, eq91 and M1 is 5663, 5607, 5537 and 5537, while the number of fixed atoms is 3002, 2964, 2714 and 3074, respectively). Finally, the QM region comprised 65 atoms, with a total charge of –1, and included the two magnesium ions, all the residue side chains and water molecules belonging to their first coordination spheres (*i.e.* the phosphate groups from the ATP molecule, the side chain of residues Asn171 and Asp184, and three crystallographic waters), the Lys168 side chain, and all the atoms involved in the breaking/forming of chemical bonds (that is, besides the γ-phosphate group of the ATP molecule already included, the Asp166 side chain and, obviously, the $Ser17_{Kemptide}$ side chain; see schemes in Figure 1). All cuts were applied in aliphatic C-C bonds, except that performed in the C5'-O5' bond of the ATP ribose, which separates the complete triphosphate tail from the

adenosine nucleoside moiety (the latter was treated at the MM level in order to keep the QM region computationally affordable). A larger QM region was tested including therein other enzyme residues interacting with ATP and Kemptide, but the new QM/MM partition caused no change in the calculated barrier heights for the phosphoryl transfer. Therefore, we decided to keep the original QM/MM region, computationally more convenient. The Figures showing molecular structures were generated using the VMD version 1.8.7.[54]

All the QM/MM calculations were performed with the modular program package ChemShell,[55] using TURBOMOLE[56] to obtain the quantum mechanical (QM) energies and gradients employing a DFT method. Specifically, the QM region was treated with the B3LYP[57-59] functional, expanding wave-functions by means of Pople's 6-31+G(d) basis set.[60, 61] The energies and gradients for the MM region were evaluated by DL_POLY,[62] which was accessed through the ChemShell package using the CHARMM22 force field.[63, 64] In previous studies, we have shown that the B3LYP functional was a good choice for phosphorous-containing systems,[65] and that the B3LYP/6-31+G(d)/CHARMM level of calculation provided good geometries and energies at reasonable computational time.[36] An electronic embedding scheme was adopted in the QM/MM calculations with the MM point charges being incorporated into the one-electron Hamiltonian during the QM calculation. No cutoffs were introduced for the non-bonding MM and QM/MM interactions. According to the QM region defined above, six hydrogen link atoms were used to connect the QM and MM parts of the system.[66] The QM/MM interaction energy was determined with the charge-shift approach.[67] Energy minimizations were performed employing the Limited-memory Broyden-Fletcher-Goldfarb-Shanno (L-BFGS) algorithm,[68] while the transition state searches were carried out by means of the microiterative optimizer[69, 70] combining the L-BFGS and the partitioned rational function optimizer (P-RFO).[71] Both algorithms are implemented in the HDLCopt[70] module of ChemShell.[55] The characteristic single imaginary frequency and the chemically proper transition vector were confirmed for all reported transition states by means of frequency calculations for the QM region. Natural population analysis (NPA)[72] charges were determined from QM/MM calculations. More accurate energy evaluations were obtained by single-point energy calculations at the MP2[73]/cc-pVTZ[74]/CHARMM level of theory.

For all the starting structures, an initial QM/MM optimization was carried out to avoid any distortions caused by the force field used along the previous MD simulations and to eliminate any artifacts related with the building up of the molecular system. Afterwards, the potential energy profiles were scanned by constrained QM/MM optimizations along a reaction coordinate in steps of 0.2 Å, according to the equation properly defined for the phosphoryl

transfer following a concerted loose mechanism (equation that involves the two anti-symmetrical combinations of the bonds to be broken and formed):

$$R4 = r_1 - r_2 + r_3 - r_4 \quad (1)$$

where $r_1$ is the O3βATP–PγATP distance, $r_2$ is the OγSer17–PγATP distance, $r_3$ is the OγSer17–HγSer17 distance, and, finally, $r_4$ is the Oδ2Asp166–HγSer17 distance (see Figure 1B). The potential energy profiles have been calculated going forwards and backwards (from reactants to products and *vice versa*) until convergence to the reaction path with the lowest potential energy barrier is reached. This provided us with appropriate starting structures for subsequent full QM/MM optimization of all stationary points (*i.e.* reactant complex, transition state, and product complex).

For each initial model, the optimized product of the phosphoryl transfer path (named, from now on, as P1) was then used as the starting structure for scanning the reaction path corresponding to the second step of the concerted loose mechanism, that is, the proton (HγSer17) transfer from the catalytic base Asp166 to any of the Oγ atoms of the phosphoryl group already transferred to the substrate Ser17. Thus, again in steps of 0.2 Å, we performed constrained QM/MM optimizations along the reaction coordinate defined as:

$$R2 = r_4 - r_5 \quad (2)$$

where $r_5$ is the *Oi*γATP–HγSer17 distance (*i* = 1, 2, 3; see Figure 1C). When it was possible to simulate a converged proton transfer path, we confirmed that it yielded the same optimized P1 structure – both geometrically and energetically – as the preceding phosphoryl transfer path (that is, we have ensured that both reactive paths are connected through the same molecular complex). From the suitable structures, we then characterized the final product complex by full QM/MM optimization and performed a microiterative QM/MM TS search, as described above.

**Results and Discussion**

As already described in the Models and Methods section, to simulate the concerted loose mechanism we have used as starting point the same structures (named eq21, eq55, eq91, and M1) as the ones taken when analyzing the concerted tight mechanism,[38] although as we will explain below, not all of them led to successful reaction channels.

***Phosphoryl transfer step***

*Exploration of the potential energy surface*

From each initial structure chosen in this work, we have attempted to simulate the entire concerted loose mechanism for a wild type PKA-$Mg_2$ATP-Kemptide model at the B3LYP/6-31+G(d)/CHARMM level. However, only one initial structure allowed us to define an acceptable profile (*i.e.* with appropriate potential energy barriers) for both the phosphoryl and proton transfer steps: the eq21 structure. In this section we analyze the phosphoryl transfer reaction path.

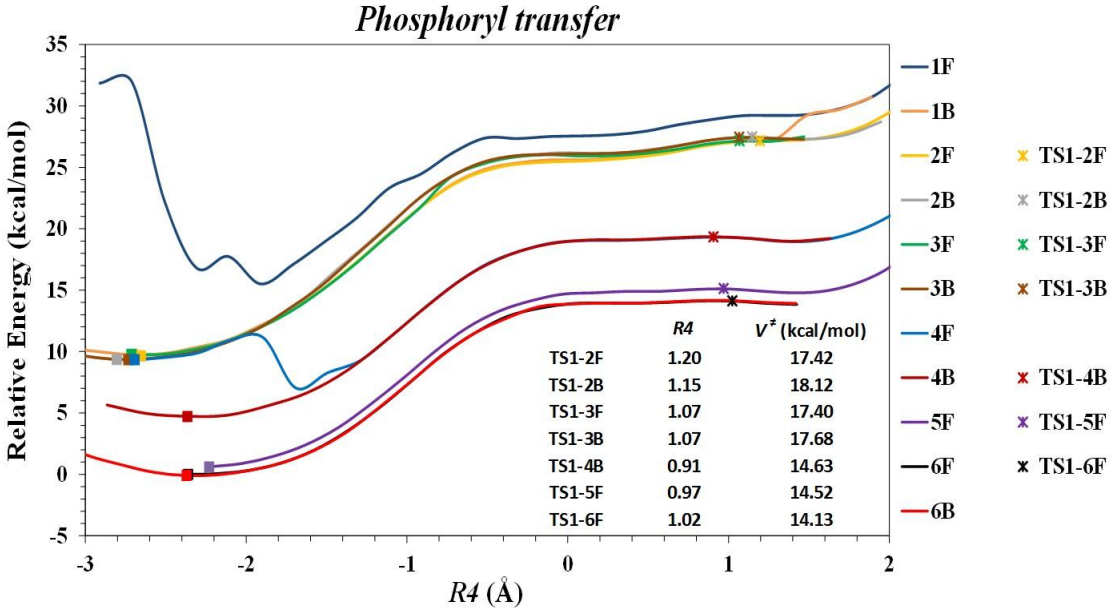


**Figure 2.** B3LYP/6-31+G(d)/CHARMM potential energy profiles along the *R4*-reaction coordinate for the phosphoryl transfer step. The location of the minimum potential energy stationary points and the transition state structures is indicated with solid squares and with asterisks, respectively, following the color code of the potential energy profiles.

The potential energy profiles calculated for this first step are shown in Figure 2. As indicated in the Models and Methods section, those potential energy profiles have been calculated going forwards and backwards (from reactants to products and *vice versa*) until convergence to the reaction path with the lowest potential energy barrier is reached. In this particular case, 11 potential energy profiles were computed (5 forward and 6 backward). Eight of those potential energy profiles are reaction paths for the phosphoryl transfer step with the corresponding transition state structures but three of them are not.

As can be seen in Figure 2, the first forward and backward potential energy profiles (1F and 1B, respectively) cannot be considered reaction paths because the corresponding transition states could not be located. In contrast, the potential energy profiles named as 2F, 2B, 3F, and

3B are phosphoryl transfer reaction paths with a transition state structure which has been located for each one using as starting point of the TS search the structure corresponding to the reaction path energy maximum. Those TS structures have been denoted, accordingly, TS1-2F, TS1-2B, TS1-3F and TS1-3B in Figure 2. The potential energy barriers for the phosphoryl transfer step at those four transitions states relative to their respective minima are quite similar (values in between 17.4 and 18.1 kcal/mol) and they are located at *R4* values in between 1.07 and 1.20 Å (see Figure 2). Of the next five potential energy profiles only the one denoted as 4F cannot be considered as a reaction path for the phosphoryl transfer process. In contrast, the potential energy profiles named as 4B, 5B, 6F and 6B are reaction paths with their corresponding transition state structures (TS1-4B, TS1-5B, TS1-6F and TS1-6B, although the latter is not shown in Figure 2 because it coincides geometrically and energetically with TS1-6F). Those last transition states are located somewhat earlier on the *R4*-reaction coordinate and their corresponding potential energy barriers are lower (values in between 14.1-14.6 kcal/mol) in comparison with the previous set of transition states. Following this strategy the finally obtained reaction path with the lowest potential energy barrier is the one denoted as 6F (as indicated above, 6B in the backward direction is coincident with 6F). The TS1-6F structure imposes the lowest barrier for the phosphoryl transfer step with a value of 14.1 kcal/mol which practically matches the value corresponding to the potential energy maximum so validating the convergence of the reaction path. The analysis of this TS structure reveals that in the concerted loose mechanism the proton is not promptly shifted from the substrate hydroxyl to the nascent phosphoryl group, rather it is delivered to the carboxylate group of the highly conserved Asp166 that is acting as a concerted catalytic base. This proton transfer takes place without additional energy cost, since while the formation of the bond between the γ-phosphoryl group and the serine side chain progresses, the acidity of the serine hydroxyl group increases, in turn, that proton transfer increases the nucleophilicity of the substrate oxygen atom during its attack on the electrophilic Pγ.

As the rest of reaction paths, the 6F pathway describes an endoergic step, with the product of the phosphoryl transfer laying 13.8 kcal/mol in potential energy over the reactant complex (so the potential energy barrier for going back to the reactant complex is really small, 0.3 kcal/mol). The reactant complex stationary point structure ($R_a$) was obtained by means of full DFT/MM structural optimization of the 6F reaction path's lowest-potential energy geometry. The same procedure, but with a product-like geometry (*R4* ≥ 1.0 Å, *i.e.* the ADP/phosphorylated-substrate region) as starting point, was used to localize a phosphoryl transfer product structure (P1). From those directly located stationary points we have

obtained an endoergicity of 13.8 kcal/mol. This value matches that obtained from the analysis of the reaction path, so confirming again its convergence.

At this point we should discuss the physical meaning of the stationary points located along the 6F pathway. Both TS1 and P1 are mathematically well characterized transition state and product structures, respectively, in what refers to the gradient and number of negative eigenvalues of their Hessian matrices, according to what is described in the Models and Methods section. However, the very small depth of P1 well indicates that P1 cannot be considered as an actual minimum energy structure from the chemical point of view. As a matter of fact, the inclusion of the zero-point energy (ZPE) correction shows that the lowest vibrational level of P1 would already overcome the energy barrier imposed by TS1 (although it has to be noted that the harmonic approach used to calculate this ZPE is not adequate for such a shallow well). Anyway, beyond the strict mathematical topology of this region of the potential energy surface, we can conclude that our results indicate the existence of a very flat potential energy region corresponding to the zone where the migrating phosphoryl group is already forming its new bond with the OγSer17 (see below). P1 turns out merely to be a structure more advanced than TS1 along the reaction coordinate that can be useful to describe how the chemical process advances. This makes evident that this region does not contain the final stable phosphokemptide product yet.

The eq21 initial structure and the converged reaction path share in common a characteristic that resembles the trend already found for the concerted tight mechanism. That is, the Thr201 residue anchors along the phosphoryl transfer step both Asp166 and Lys168 via hydrogen bonds to their side chains, and thus, we can hypothesize that the presence of the Asp166-Thr201-Lys168 catalytic triad stabilizes the concerted loose phosphoryl transfer transition state. This will be further analyzed below with respect to the interaction distance analysis. In contrast, the potential energy profiles obtained from the other initial structures, *i.e.* eq55, eq91 and M1, present maxima as high as 49.3, 38.7 and 23.7 kcal/mol at *R4* values of 1.27, 1.20 and 0.52 Å, respectively. In view of these high potential energy values in comparison with the phenomenological free energy barrier for the phosphoryl transfer process, we have discarded these reaction channels. The visual inspection of the reactant structures allows us to hypothesize about the reason for the unsuccessfulness of the mentioned structures. In all of them (eq55, eq91 and M1) and in comparison to the successful eq21 structure, the Thr201 residue is further away from Asp166, and in the eq91 and M1 structures also from the Lys168 residue (see Table 1). On the other hand, in the eq55 structure, the value of the dihedral angle between Asp166 and the PγATP is significantly different from such geometric parameter's value in the eq21 structure. Moreover, this geometric disposition is maintained along the

whole phosphoryl transfer profiles and indicate a clear difference in the orientation and interaction of the catalytic residues between the eq21 structure and the other models. In the case of eq55, corresponding to the highest potential energy profile obtained, the loose interactions between the active site residues result in a longer distance between the reactant moieties, and the potential energy profile exploration had to be initiated at *R4* values around -4 Å. In the well-formed catalytic triad (that in our case only appears in the eq21 structure), Thr201 anchors both Asp166 and Lys168, giving to Asp166 the proper orientation to act as an acid-base catalytic residue, and to Lys168 the proper position to bridge the reactant moieties together, that is, the Ser17 residue side chain and the γ-phosphoryl group of ATP. Therefore, from the analysis just described above, we conclude that the unsuccessful phosphoryl transfer profiles from eq55, eq91 and M1 initial structures, might be associated to a distance around 4 Å between Asp166 and Thr201 residues which prevents the formation of the catalytic triad. Those results are in agreement with experimental observations.[42]

**Table 1.** Interaction distances (in Å) within the three residues of the catalytic triad at the four initial structures. Intermolecular dihedral (in degrees) between Asp166 and PγATP.

| | eq21 | eq55 | eq91 | M1 |
|---|---|---|---|---|
| Oγ1Thr201-Oδ1Asp166 | 2.73 | 3.78 | 4.09 | 4.01 |
| Oγ1Thr201-NζLys168 | 2.79 | 2.75 | 3.66 | 3.32 |
| Oδ2Asp166-NζLys168 | 4.15 | 2.81 | 3.46 | 3.55 |
| Oδ2Asp166-OγSer17 | 2.64 | 3.50 | 2.84 | 2.93 |
| NζLys168-O2γATP | 3.41 | 3.42 | 2.97 | 2.83 |
| NζLys168-OγSer17 | 2.67 | 3.03 | 2.83 | 2.83 |
| $dihedral_{CβAsp166\text{-}CγAsp166\text{-}Oδ2Asp166\text{-}PγATP}$ | 144.12 | -78.27 | 133.15 | 129.60 |

While performing the exhaustive exploration along the *R4*-reaction coordinate (Figure 2) in order to accomplish convergence to the reaction path with the lowest potential energy barrier, a different or geometrically distinguishable reaction zone was reached. This structural change is the cause of the energetic bump observed when following the potential energy profile denominated as 4F (see Figure 2), and it is a molecular rearrangement that it is maintained in the following reaction paths (that is, 4B, 5B, 6F and 6B). From now on we will refer as $R_a$ to the reactant complex stationary point of the 6F reaction path after the structural rearrangement, and $R_b$ will denote the reactant complex stationary point of the 3F reaction path before the structural change.

As shown in Figure 3, the main geometric difference between the $R_a$ and $R_b$ reactant complexes is the relative distance of the Lys168 side chain ε-amino group to the carboxylate group of Asp166 side chain and to the O2γ atom of the terminal phosphate of ATP, along with the Lys168 side-chain dihedral Cγ-Cδ-Cε-Nζ. In the reduced view of the active site at $R_a$ shown in Figure 3A, Lys168 is in a more distant position to such groups than in the reduced view corresponding to $R_b$ (Figure 3B). The Lys168 dihedral Cγ-Cδ-Cε-Nζ takes values of 161.4° and 74.7° at Ra and $R_b$, respectively, that correlate with the different orientation of Lys168 side chain in the two minima. Those differences are maintained along the whole phosphoryl transfer profiles. Therefore, we can conclude that the phosphoryl transfer step is energetically favored –a potential energy barrier about 3 kcal/mol lower– as Lys168 is further away from Asp166 and the O2γ of ATP. This result can be seen as contradictory to the proposed catalytic role of the catalytic triad, but one has to realize that, first, the formation of the catalytic triad, that is, a bridge between Lys168 and Asp166 residues through Thr201 residue, is independent of the Asp166-Lys168 distance; and second, a too short distance between Asp166 and Lys168 reduces the basic character of Asp166 and might be the cause of the higher potential energy barrier of the profile related to $R_b$. In addition, and as will be discussed below, the Lys168-O2γATP distance seems to determine the success of the overall reaction channel.

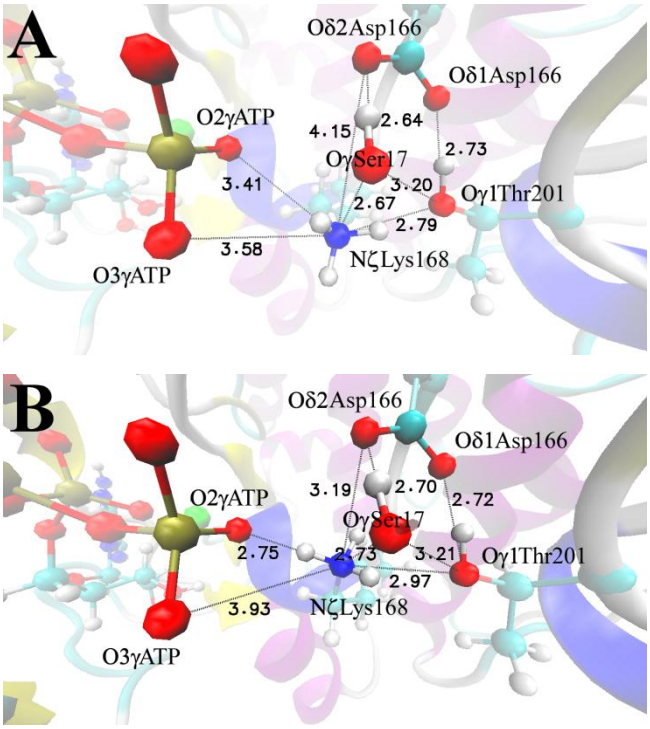


**Figure 3.** Hydrogen bond interactions and relevant heavy-heavy atom distances involving the three residues of the catalytic triad Asp166-Thr201-Lys168 and the O2γATP, O3γATP and OγSer17

atoms: A) At the $R_a$ minimum potential energy structure; B) At the $R_b$ minimum potential energy structure.

In summary, from the $R_a$ structure we have obtained the lower potential energy barrier at the B3LYP/6-31+G(d)/CHARMM level for the phosphoryl transfer step involved in the concerted loose mechanism. So, from now on, only the results obtained from this structure will be reported and discussed in the main text, unless stated otherwise. To complete the energetic analysis we have performed single-point energy evaluations at the MP2/cc-pVTZ/CHARMM level of theory on the B3LYP/6-31+G(d)/CHARMM stationary points. The high level potential energy barrier and reaction potential energy values (10.9 kcal/mol and 10.4 kcal/mol, respectively) are somewhat lower than the DFT ones.

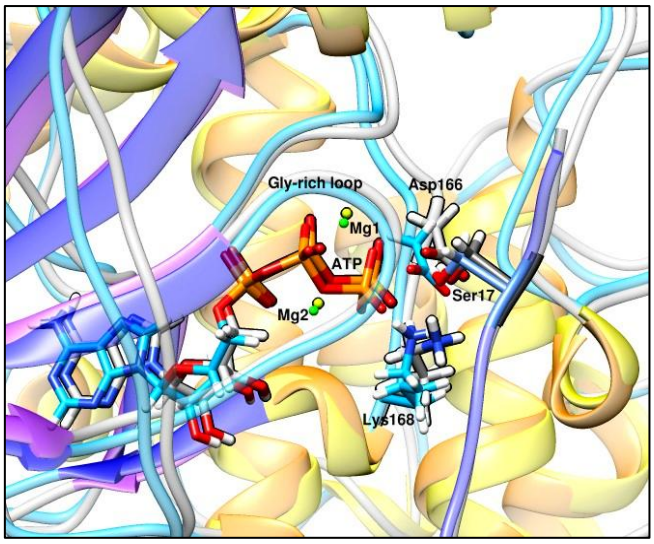


**Figure 4.** Overlay between 1CDK-Kemptide model at $R_a$ and that obtained as a preliminary result from the 1ATP-Kemptide model following the same *in silico* methodology.

*Structural analysis comparison between theory and experiments*

The increasing number of crystallographic structures available in the Protein Data Bank for diverse complexes of the wild-type PKA with several ligands give us the opportunity to compare some of our theoretically localized stationary point structures (reactants, transition state and products) with crystallographic models of the different steps of the enzyme's catalytic cycle. This is specially applicable to the models based on the 1ATP crystallographic structure,[48] because Taylor and coworkers have crystallized PKA complexes of the same species (*Mus musculus*) that serve as transition state and ATP-hydrolysis product analogs, with ID numbers 1L3R[44] and 4DH5,[43] respectively. However, the model used in this study comes from the *Sus scrofa* PKA (1CDK crystallographic structure).[49] In Figure 4 we show the structural

proximity between the reactant complex ($R_a$) defined in this work for the 1CDK-Kemptide model and that obtained as a preliminary result from the 1ATP-Kemptide model following the same *in silico* methodology (*i.e.* MD simulation, specific snapshot selection, concerted loose reaction path scanning and stationary point localization by means of constrained and full B3LYP/6-31+G(d)/CHARMM optimization, respectively). The RMSD between both structures calculated for all backbone atoms within a sphere of 15 Å centered at the PγATP atom is 0.924 Å. Such a small value confirms the similarity between the two compared stationary points.

The significance of this similarity is that it allows us to use the *Mus musculus* PKA crystals as a reference for our theoretical 1CDK-derived model. Consequently, we present in Figures 5A and 5B the overlay images of our theoretically determined transition state and product complex of the phosphoryl transfer step and the corresponding crystallographic structures.

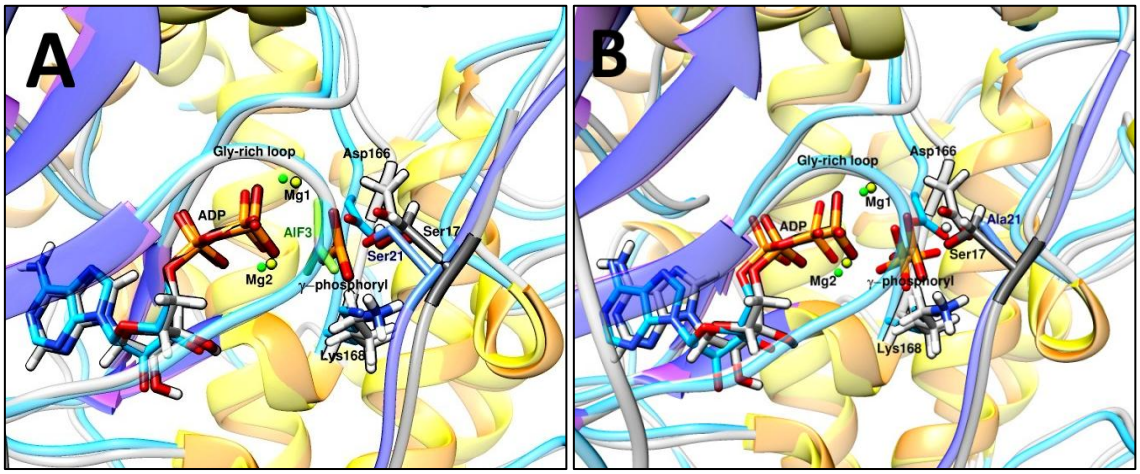


**Figure 5.** A) Overlay between the 1CDK-Kemptide model at TS1 and the transition state analog crystallographic structure (1L3R): B) Overlay between the 1CDK-Kemptide model at P1 and the ATP-hydrolysis product analog crystallographic structure (4DH5).

As for the phosphoryl transfer transition states comparison (Figure 5A), the RMSD between both structures was calculated. The small value obtained of 0.764 Å reflects the similarity between the crystallographic and the model-based structures. The most notable difference entails the relative position of the metal-trifluoride that mimics the γ-phosphoryl in the 1L3R transition state analogue structure (TSA),[44] and that of the γ-phosphoryl in our calculated geometry (TS1). In the TSA, the metal-trifluoride has a planar configuration and is in an equidistant position (about 2.3 Å) to the donor and recipient oxygen atoms (O3β of ADP and Oγ of Ser21, respectively), which in turn occupy the apical positions of the trigonal bypiramidal coordination of the metal atom. In the TS1, the γ-$PO_3$ group also has a planar configuration with the phosphorous atom bearing a similar trigonal bypiramidal coordination, but the

distances to the donor and recipient oxygen atoms are 2.84 and 1.86 Å, respectively (see Table 2). The foregoing points towards a more loose character for TS1 than for TSA.

Regarding the 4DH5 product analog, Kovalevsky *et al.*[43] pointed out that it represents a transient stage in the reaction after the hydrolysis of ATP but before the transfer to the substrate residue of the released phosphate group. This group in turn imposes an electrostatic effect on the surrounding residues due to its large negative charge. This fact may explain the difference in the relative positions of the highlighted residues in the superposition of such product analog and our calculated P1 structure (Figure 5B) although the calculated RMSD value is quite small (0.691 Å). Meaningfully, within the active site of both structures, the nucleotide moieties and residues' side chains have the same orientation and, consequently, are held together by the same hydrogen-bonding interactions.

*Geometric analysis of the main interactions along the phosphoryl transfer step*

Next, in order to rationalize the calculated potential energy differences between the localized stationary points, we will compare the evolution of the main interaction distances along the reaction profile (Figure 2) that represents the phosphoryl transfer path.

The values corresponding to the distances involved in the *R4*-reaction coordinate are listed in Table 2. In the optimized structure of $R_a$ the PγATP-OγSer17 distance was found to be 3.48 Å in our calculations, an intermediate value among those obtained from MD simulations,[31, 32] QM cluster calculations,[31] and QM/MM approaches[32, 34] of the phosphorylation reaction in other catalytic subunit models of PKA with other substrates. The length of the ATP O3β-Pγ bond, 1.77 Å, is in good agreement with the value defined as "natural" by Valiev *et al*.[34] in the ATP-Mg complex in the PKA active site within the limits of DFT description. Furthermore, prior the phosphorylation reaction, the angle O3βATP-PγATP-OγSer17 is almost linear (176.9°), thereby confirming the in-line nature of the phosphoryl transfer mechanism observed in PKA. On the other hand, as expected for a concerted loose mechanism conducive initial structure, the hydroxyl group of the Ser17 side chain is rotated toward –and interacting with, through a 2.64 Å hydrogen bond– the carboxylate group of Asp166 (angle OγSer17-HγSer17-Oδ2Asp166 of 176.9°), forming a 2.67 Å hydrogen bond with the Nζ atom of the ammonium side chain of Lys168, too (Figure 3A).

The *R4* interaction distances (Table 2) confirm the concerted loose character for the phosphoryl transfer transition state (TS1), so that the segment of the reaction coordinate that describes the evolution of $R_a$ to TS1 mainly involves the movement, up to an asymmetrical position, of the terminal phosphoryl group, from the β-γ bridging oxygen of ATP to the substrate hydroxyl oxygen. Specifically, in the TS1 structure, the ATP O3β-Pγ bond is already

broken (2.84 Å) and the bond between the P atom of the phosphoryl transferring group and the O atom of the nucleophilic hydroxyl group of substrate serine is almost formed (1.86 Å). On the other hand, the position of the HγSer17 between the donor OγSer17 and the acceptor Oδ2Asp166 (distances of 1.22 and 1.18 Å, respectively) clearly indicates that such proton transfer is in its halfway stage and occurs after the nucleophilic displacement. Frequency calculations within the QM/MM description of the system confirmed a single imaginary frequency mode of 160i $cm^{-1}$, whose transition vector shows a contribution from the evolution of the bonds O3βATP-PγATP and PγATP-OγSer17, and the movement of the serine hydroxyl hydrogen towards the carboxylate side chain of Asp166. It is important to note that in TS1 the γ-phosphoryl group has a planar configuration and the angle O3βATP-PγATP-OγSer17 retains its linear character (176.6°). That is, the reaction proceeds through a trigonal bipyramidal pentacoordinated TS1.

**Table 2.** B3LYP/6-31+G(d)/CHARMM interaction distances (in Å) involved in *R4* and *R2* for the catalytic core at the reactant Michaelis complexes, transition states, and product structures for the phosphoryl and the proton transfer steps. Intermolecular dihedral (in degrees) between Asp166 and O2γATP.

| | | Phosphoryl transfer | | Proton transfer | |
|---|---|---|---|---|---|
| | $R_a$ | TS1 | P1 | TS2 | P2 |
| O3βATP-PγATP | 1.77 | 2.84 | 2.91 | 3.05 | 2.88 |
| PγATP-OγSer17 | 3.48 | 1.86 | 1.80 | 1.70 | 1.68 |
| OγSer17-HγSer17 | 0.99 | 1.22 | 1.39 | 2.15 | 2.43 |
| Oδ2Asp166-HγSer17 | 1.65 | 1.18 | 1.07 | 1.01 | 1.80 |
| O2γATP- HγSer17(Asp166) | 3.39 | 2.81 | 2.85 | 1.79 | 0.99 |
| $dihedral_{Asp166(Cβ\text{-}Cγ\text{-}Oδ2)\text{-}O2γATP}$ | 121.07 | 122.96 | 124.18 | 178.37 | -173.79 |

Energetically, as mentioned above, P1 is scarcely 0.3 kcal/mol below TS1 (Figure 2) and, consequently, this point is structurally very similar to TS1 in what concerns the phosphoryl transfer, with a PγATP-OγSer17 distance just 0.06 Å shorter and maintaining the same trigonal bipyramidal pentacoordination. In contrast, the structural quantities related to the proton transfer from the hydroxyl group of Ser17 to the carboxylate group of Asp166 undergo the most significant changes as the TS1 evolves to P1 along this flat potential energy region. In the P1 structure, the protonated Asp166 side chain establishes a short hydrogen bond with the now phosphorylated substrate oxygen (Oδ2Asp166–OγSer17 distance of 2.45 Å and a hydrogen bond angle of 165.7°), and the HγSer17 is 2.85 and 3.11 Å away from –and not directed towards– O2γATP and O1γATP, respectively. It is noteworthy that the PγATP–OγSer17

and Oδ2Asp166–HγSer17 bond distances are slightly longer than those reported previously for the same intermediate product structure of 1ATP-SP20 based PKA models.[32, 34]

Hereinafter, we will analyze the interactions made by enzyme residues with each other and with the ligands (substrate Kemptide and ATP), which have been collected in Table 3. In addition, Figure 6 is a reduced view of the active site at TS1 where we can distinguish the location of the residues involved in the interaction distances commented in the following paragraphs.

The first twelve rows of Table 3 are dedicated to the interaction distances of residues that comprise the triad Asp166-Thr201-Lys168, whose catalytic role has already been mentioned above for the concerted loose mechanism, and highlighted recently for the concerted tight mechanism.[38] Thr201 belongs to the peptide positioning loop of PKA, whereas Asp166 and Lys168 belong to the catalytic loop. Table 3 indicates that Thr201 forms hydrogen bond interactions with the non-proton accepting side of the carboxylate group of Asp166 side chain (Oδ1Asp166 atom) and with the ammonium group of Lys168 side chain, while interacts weakly with the substrate serine Oγ atom. The hydrogen bonds with Asp166 and Lys168 residues are maintained throughout the phosphoryl transfer reaction profile, while the interaction with the residue Ser17 of the substrate seems to decrease in going from $R_a$, passing through TS1, to P1.

**Table 3.** Selected B3LYP/6-31+G(d)/CHARMM distances (in Å) for the enzyme, nucleotide and substrate interactions at the reactant, transition states, and products structures for the phosphoryl and proton transfer steps.

| | | Phosphoryl transfer | | Proton transfer | |
|---|---|---|---|---|---|
| | $R_a$ | TS1 | P1 | TS2 | P2 |
| Oγ1Thr201-Oδ1Asp166 | 2.73 | 2.72 | 2.74 | 2.74 | 2.70 |
| Oγ1Thr201-NζLys168 | 2.79 | 2.83 | 2.85 | 2.84 | 2.71 |
| Oγ1Thr201-OγSer17 | 3.20 | 3.45 | 3.47 | 3.49 | 4.00 |
| Oδ2Asp166-OγSer17 | 2.64 | 2.39 | 2.45 | 2.80 | 3.09 |
| Oδ2Asp166-PγATP | 4.26 | 3.46 | 3.47 | 3.31 | 3.54 |
| Oδ2Asp166-OH2XWAT536 | 2.79 | 2.88 | 2.91 | 2.90 | 2.83 |
| Oδ2Asp166-NζLys168 | 4.15 | 4.58 | 4.65 | 4.49 | 4.01 |
| Oδ1Asp166-NζLys168 | 4.33 | 4.49 | 4.52 | 4.36 | 3.97 |
| NζLys168-OγSer17 | 2.67 | 3.01 | 3.02 | 3.15 | 2.86 |
| NζLys168-PγATP | 3.97 | 3.42 | 3.39 | 3.36 | 3.64 |
| NζLys168-O2γATP | 3.41 | 3.28 | 3.27 | 3.22 | 3.28 |
| NζLys168-O3γATP | 3.58 | 2.99 | 2.97 | 2.88 | 3.68 |
| Nδ2Asn171-O2γATP | 3.44 | 3.11 | 3.09 | 3.21 | 3.62 |

| | | | | | |
|---|---|---|---|---|---|
| Nδ2Asn171- Oδ2Asp166 | 3.86 | 3.99 | 4.01 | 3.15 | 3.07 |
| NζLys72-O1αATP | 2.75 | 2.75 | 2.75 | 2.75 | 2.75 |
| NζLys72-O2βATP | 2.89 | 2.86 | 2.85 | 2.85 | 2.86 |
| NζLys72-Oε2Glu91 | 2.66 | 2.68 | 2.68 | 2.68 | 2.67 |
| OγSer53-O3γATP | 2.65 | 2.64 | 2.64 | 2.64 | 2.64 |
| NSer53-O1βATP | 2.79 | 2.74 | 2.75 | 2.73 | 2.78 |
| NPhe54-O1βATP | 2.80 | 2.77 | 2.77 | 2.78 | 2.82 |
| NGly55-O1βATP | 2.88 | 2.85 | 2.84 | 2.85 | 2.88 |

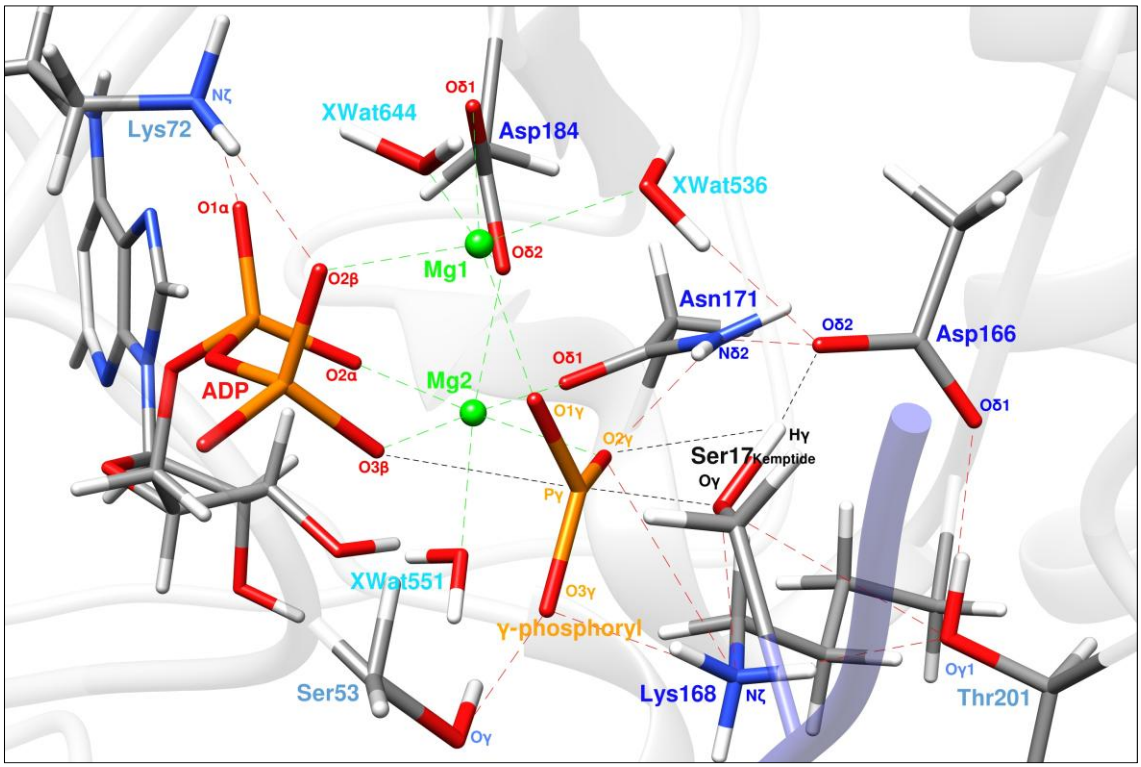


**Figure 6.** Reduced view of the active site at the TS1 structure of the phosphoryl transfer step. The most relevant interactions presented in Tables 2, 3 and 4 are depicted in broken lines.

In turn, besides the obvious and already described interaction with the nucleophilic OH group of Ser17 side chain, Asp166 also interacts via hydrogen bonds with a conserved water molecule (coordinated to the Mg1 ion). It also interacts with the conserved Asn171 residue, through its proton accepting carboxylic oxygen (Oδ2Asp166 atom). Both interactions do not show important variations along the stationary points defined from the phosphoryl transfer reaction profile. Moreover, as explained above, the Asp166 residue is detectably away (see Figure 3A) from the Lys168 ammonium group, although these two residues are anchored by the residue Thr201.

Now, let us finish the description of the three members of the catalytic triad by focusing on Lys168 interactions. Apart from its interaction with Thr201, Lys168 maintains its interaction with the OγSer17 atom, although with increasing interaction distances, in going from the reactant to the transition state and product zones. The analysis of the values reported in Table 3 for the distance NζLys168-PγATP shows that the distance of this residue to the phosphoryl group diminishes about 0.6 Å in going from reactant to product. That is, Lys168 slightly approaches the γ-phosphate group of ATP along the phosphoryl transfer step. Specifically, in $R_a$, the closest γ-oxygen atoms of ATP to NζLys168 is the O2γ atom (the one coordinated to Mg2). However, at TS1 and P1, this interaction has clearly longer distance values than the corresponding one for O3γATP, which seems to be related to the progressive distancing of the Lys168 ε-amino group from the reaction core as the phosphoryl transfer reaction occurs (see Oδ2Asp166-NζLys168 and NζLys168-OγSer17 distances in Table 3).

At this point, it is worth comparing the results obtained here with those from Montenegro et al.[36] on the same concerted loose mechanism using the 1CDK-Kemptide based PKA model. As indicated above, our previous calculations of the phosphoryl transfer reaction path were carried out at the AM1/d-PhoT/MM level with a rather rigid *R4*-reaction coordinate expression in which fixed coefficients were used to account for the contributions of the four different distances (*r1*, *r2*, *r3*, and *r4*) involved in the chemical process. The potential energy was then corrected along the reaction path by means of single point energy calculations at the B3LYP/6-31+G*/MM level. However, the DFT-corrected potential energy profile based on the weigthed-R4 reaction coordinate was so rugged that it was not possible to use it to locate the phosphoryl transfer stationary points. Finally, by means of a strategy consisting in the calculation of a corrected 2D-surface obtained from the difference between the high level (HL) B3LYP/6-31+G(d)/MM and the low level (LL) AM1/d-PhoT/MM 2D-PESs, and by fitting these difference values through a two dimensional cubic spline function, the three stationary points, reactant (R), transition state (TS) and product (P), were located. The nature of the concerted loose transition state is the same in both studies. So, the interaction distances O3βATP-PγATP and PγATP-OγSer17, involved in the *R4*-reaction coordinate, at TS and TS1 are practically identical. However, the dual-level potential energy barrier and reaction energy values of the phosphoryl transfer process in Montenegro et al.,[36] differ from the converged energetic values obtained in the present study at the B3LYP/6-31+G*/MM level with the new flexible R4-reaction coordinate. The reason is that several interactions that have been identified as very important for the energetics of the phosphoryl transfer process on the B3LYP/6-31+G*/MM potential energy surface (PES) were not present on the DFT-corrected AM1/d-PhoT/MM PES. For instance, the triad Asp166-Thr201-Lys168 was not correctly formed in the structures along

the phosphoryl-transfer reaction path of our previous study. Moreover, when comparing the Lys168 hydrogen bond interactions at the TS1 and P1 structures with those at the corresponding structures, TS and P, respectively, in Montenegro *et al*.,[36] it is clear that in the ternary structures obtained in the present study the Lys168 amino group is more distant from the carboxylate group of Asp166 and the hydroxyl group of Ser17. The foregoing, besides enhancing the basic character of Asp166, also increases directly the nucleophilicity of the Ser17 attacking oxygen atom, then promoting the phosphoryl transfer reaction. Moreover, such configuration of the Lys168 side chain within the active site, allowed the simulation of the final step of the catalytic mechanism, in which the protonation of the phosphorylated product by Asp166 takes place, something that has been carried out for the PKAc-$Mg_2$ATP-Kemptide system for the first time in this study. Therefore, the NζLys168-O2γATP distance is longer at the P1 structure than at the P structure, so the basic character of the O2γATP atom is stronger in the former, such that it can really act –in the phosphoryl group already transferred to the substrate Ser17– as the acceptor oxygen for the final proton transfer step.

Following with the analysis of Table 3, we will now focus on the interactions that hold and stabilize the nucleotide moieties within the active site. The O1γATP atom has no interaction apart from being one of the ligands in the Mg1 coordination sphere. The O2γATP forms a hydrogen bond with the Nδ2Asn171 atom (interaction which is strengthened as the phosphoryl transfer reaction takes place), the interaction mentioned above with Lys168, and, in addition, it belongs to the coordination sphere of Mg2. The O3γATP oxygen also interacts via hydrogen bond with the side chain OH of Ser53, located in the glycine-rich loop (a flap-like hairpin structure spanning residues 49-57, of which three are Gly residues, acting as a lid for the catalytic site cavity).[36] Another oxygen atom of ATP is responsible of other interactions with the glycine-rich loop, the O1βATP atom, which interacts with the main chain nitrogen atoms of Ser53, Phe54, and Gly55 residues. Finally, both O2β and O1α atoms of ATP form hydrogen bonds with the amino group of Lys72, which is also hydrogen bonded to the carboxylic oxygen of Glu91.

Regarding both $Mg^{2+}$ ions within their corresponding metal-binding site, the Mg1 ion binds the 2β- and 1γ-oxygens of ATP, the Asp184 side chain in a bidentate fashion, and two conserved water molecules, while the Mg2 ion binds the 2α-, 3β- and 2γ-oxygens of ATP, a single carboxyl oxygen of Asp184, and the side chain carbonyl oxygen of Asn171. Specifically, Table 4 indicates that the metal ions' octahedral coordination scheme does not significantly vary along the phosphoryl transfer reaction, with the exception of the O3βATP and O2γATP interaction distances for the Mg2 ion. As described for the concerted tight mechanism,[38] concurrently with the cleavage of the β-γ phosphoanhydride bond of ATP due to the

nucleophilic attack of OγSer17 on PγATP, the nascent and leaving ADP moiety is stabilized by the increased interaction with the Mg2 metal ion. That is, the O3βATP-Mg2 interaction is strengthened and, consequently, its distance shortened during the phosphoryl transfer step. Simultaneously, as a result of the movement of the γ-phosphoryl group almost 2 Å towards Ser17, in both the transition state and product regions the O2γATP-Mg2 distance increases almost ten percent of its initial value.

**Table 4.** Interaction distances (in Å) between the two Mg ions and the ligands of their corresponding coordination spheres along the phosphoryl and proton transfer steps.

| | | Phosphoryl transfer | | Proton transfer | |
|---|---|---|---|---|---|
| | $R_a$ | TS1 | P1 | TS2 | P2 |
| Mg1-O2βATP | 2.13 | 2.04 | 2.04 | 2.03 | 2.05 |
| Mg1-O1γATP | 2.06 | 2.13 | 2.12 | 2.11 | 2.13 |
| Mg1-Oδ1Asp184 | 2.23 | 2.29 | 2.31 | 2.34 | 2.27 |
| Mg1-Oδ2Asp184 | 2.23 | 2.19 | 2.18 | 2.21 | 2.22 |
| Mg1-OH2XWAT536 | 2.12 | 2.18 | 2.18 | 2.18 | 2.19 |
| Mg1-OH2XWAT644 | 2.07 | 2.07 | 2.07 | 2.07 | 2.06 |
| Mg2-O2αATP | 2.00 | 2.06 | 2.06 | 2.07 | 2.02 |
| Mg2-O3βATP | 2.29 | 2.04 | 2.04 | 2.02 | 2.01 |
| Mg2-O2γATP | 2.02 | 2.20 | 2.21 | 2.44 | 2.48 |
| Mg2-Oδ2Asp184 | 2.11 | 2.10 | 2.10 | 2.08 | 2.08 |
| Mg2-Oδ1Asn171 | 2.01 | 2.10 | 2.10 | 2.11 | 2.09 |
| Mg2-OH2XWAT551 | 2.13 | 2.16 | 2.17 | 2.16 | 2.14 |

***Proton transfer step***

*Exploration of the potential energy surface.*

As seen above, P1 does not correspond to a stable structure. An additional chemical step is required to reach a stable phosphokemptide. In this section, the potential energy profile at the B3LYP/6-31+G(d)/CHARMM level corresponding to the proton (HγSer17) transfer from the Asp166 residue to the O2γATP atom of the phosphoryl group already transferred to the substrate Ser17, is described. As indicated in the Models and Methods section, this second step of the concerted loose mechanism has been calculated using the *R2* coordinate from the P1 structure. The complete potential energy profile is shown in Figure 7, and encompasses both the phosphoryl transfer and the proton transfer steps along the *R4*- and *R2*-reaction

coordinate, respectively, with the phosphorylated (P1) as a common point. It also includes the MP2/cc-PVTZ/CHARMM//B3LYP/6-31+G(d)/CHARMM single point energies for all the calculated stationary points.

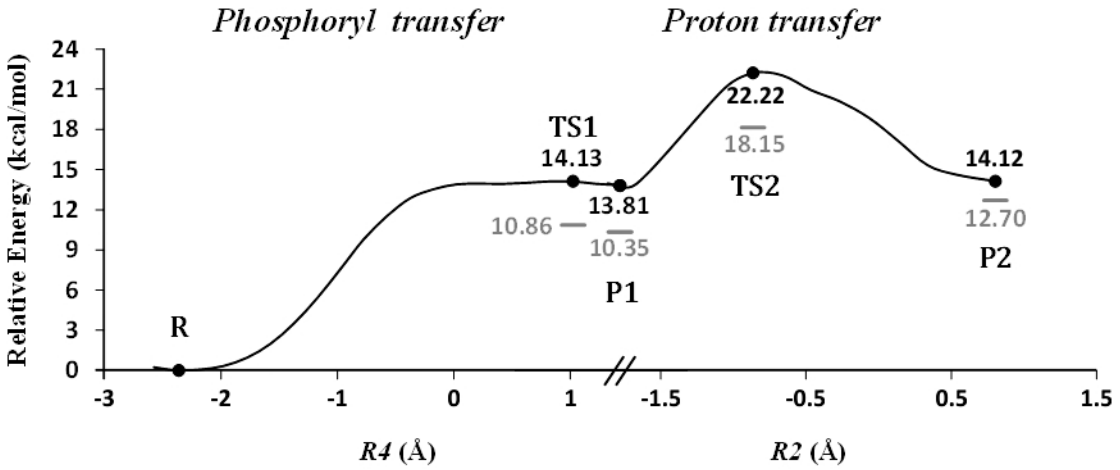


**Figure 7.** B3LYP/6-31+G(d)/CHARMM complete potential energy profile encompassing the phosphoryl and proton transfer steps along its corresponding reaction coordinate. The single-point energy results at the MP2/cc-PVTZ/CHARMM level on the B3LYP/6-31+G(d)/CHARMM stationary points structures are depicted in grey.

As can be seen in Figure 7, the proton transfer step is explored from *R2* values around -1.9 Å at the P1 zone, and the obtained potential energy profile reaches its maximum at *R2* = -0.78 Å with a potential energy value of 8.4 kcal/mol with respect to P1. It describes a nearly isoergic process. Based on the converged potential energy profile presented in Figure 7, a product-like geometry (*R2* = 0.8 Å) as starting point was used to localize a proton transfer product structure, *i.e,* the ADP/protonated-phosphokemptide structure (P2). Finally, the structure corresponding to the reaction profile's potential energy maximum was used as the starting point for the corresponding transition state (TS2) search (see Models and Methods section). The final potential energy barrier for the proton transfer step and the reaction potential energy with respect to P1 are 8.4 kcal/mol and 0.3 kcal/mol, respectively, at the B3LYP/6-31+G(d)/CHARMM level. The single-point energy calculations at the MP2/cc-PVTZ/CHARMM level on the B3LYP/6-31+G(d)/CHARMM TS2 structure, and on the P1 and P2 stationary points, give values for the potential energy barrier and reaction potential energy of 7.8 and 2.4 kcal/mol, respectively. It has to be noted that P2, which corresponds to a protonated phosphokemptide, has to be considered as the final stable product from which the phosphokemptide release occurs.

Pre-steady-state kinetics has revealed a very rapid phosphoryl transfer step in PKA using Kemptide as a substrate. From those experiments a rate constant of 500 $s^{-1}$ was determined, and the kinetic measurements indicate that the rapid phosphorylation of Kemptide occurs in a single observable step.[14] On the other hand, the phosphorylation of Kemptide by PKA was monitored[75] along time taking advantage of that the fluorescence emission spectrum of PKA is quenched differentially by ATP and ADP. Fitting of the pre-steady-state kinetic transient for Kemptide phosphorylation to a double-exponential function gave rate constants of 500 $s^{-1}$ and 60 $s^{-1}$, corresponding to a fast and a slow phase, respectively. The first phase was assigned to the evolution along time of the phosphoryl group transfer from ATP to Kemptide. The second phase was tentatively associated to a large conformational change of the enzyme, and could include the very fast phosphokemptide release. The phenomenological free energy barrier corresponding to the experimental rate constant of the first phase, obtained by applying conventional transition state theory gives a value of 13.8 kcal/mol at 300 K, which is not too far from the potential energy barrier of TS2 with respect to R calculated in this work (18.1 kcal/mol at the MP2 level; see Figure 7).

As indicated in the Introduction section, only Díaz and Field[31] have calculated the potential energy profile for the proton transfer step that protonates the phosphorylated peptide and that recovers the protonation state of the active site residues. With their cluster model, Díaz and Field[31] obtained a potential energy barrier and a reaction potential energy of 7.0 and 0.9 kcal/mol, respectively, at the B3LYP/6-31+G(d,p) level. In agreement with their results we obtain using a complete model of the ternary complex a small potential energy difference between the product complexes before (P1, deprotonated phosphoryl group) and after (P2, protonated phosphoryl group) proton transfer. In contrast, Valiev et al.[30] considered that the structure corresponding to P1 is the unique stable protonation state of the product complex of the concerted loose mechanism locating that structure 9 kcal/mol below the reactant complex in a 82-atom cluster with $HOCH_2CH_3$ as a substrate model. According to Díaz and Field,[31] that result is an artifact because the coordination sphere of the Mg1 ion was not complete in the cluster model used by Valiev et al.[30] resulting in an overstabilized product complex. More recent theoretical studies using complete models of the ternary PKA-ATP-$Mg_2$-SP20 system have also considered the P1 structure as the final protonation state of the product complex but with different results concerning the reaction energy (7.4, 9.5, and 11.9 in terms of potential energy, or -3 kcal/mol in terms of free energy).[32, 34]

*Geometric analysis of the main interactions along the proton transfer step*

Next, the potential energy differences between the localized stationary points along the proton transfer step will be analyzed by comparing the evolution of the main interaction distances along the reaction profile (Figure 7) as it has been done for the phosphoryl transfer path.

The main geometric variables involved in the *R2* coordinate are given in Table 2 and the structure of TS2 is depicted in Figure 8. It can be inferred by inspection of the structural evolution that the potential energy barrier corresponds to the rotational movement of the protonated carboxyl group of the Asp166 residue which displaces from a location with a dihedral (Asp166(Cβ-Cγ-Oδ2)-O2γATP) value of 124.18° at P1 to 178.37° at TS2 reaching a configuration more suitable for proton transfer (see Figure 8). Concomitant with the rotation of the Asp166 side chain, the O2γATP-HγSer17(Asp166) distance decreases from 2.85 Å at P1 to 1.79 Å at TS2 whereas the OγSer17-HγSer17 distance increases from 1.39 Å at P1 to 2.15 Å at TS2. However, the proton transfer has not begun yet at TS2 being the distance Oδ2Asp166-HγSer17 of only 1.01 Å. In fact, the actual proton transfer from the protonated Asp166 to O2γATP begins rather late on the reaction pathway (*R2* around -0.27 Å) in the downhill region quite close to the P2 product structure.

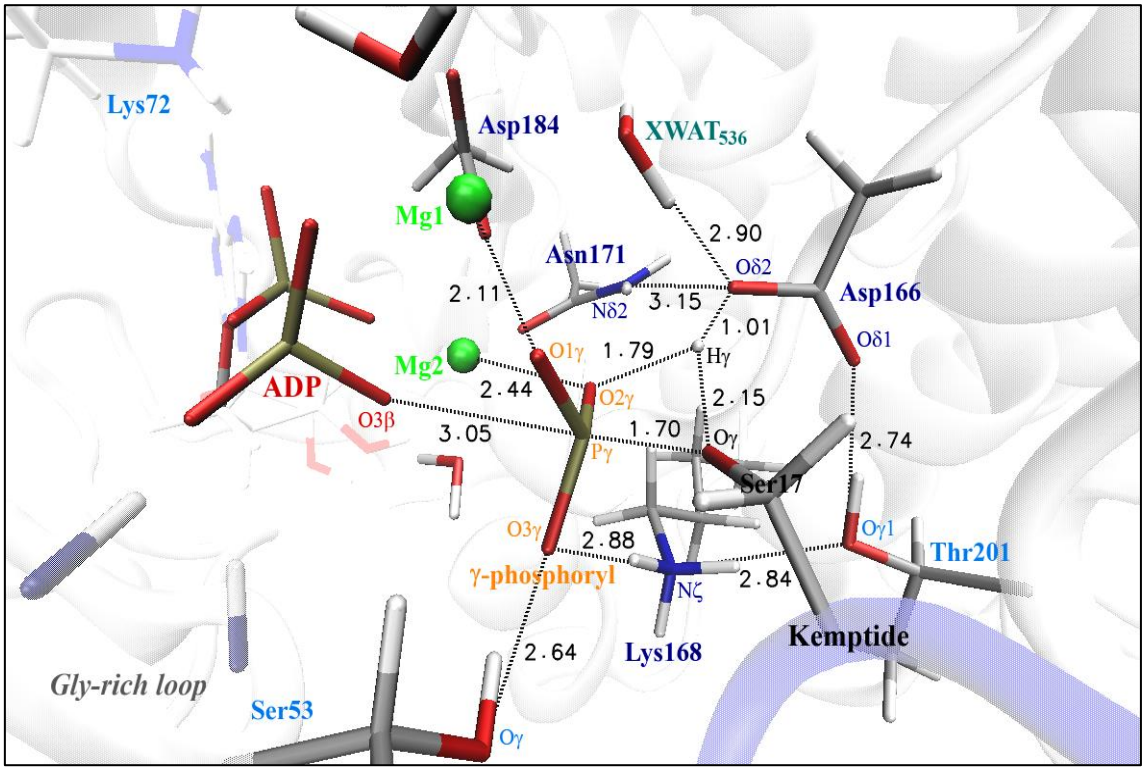


**Figure 8.** Reduced view of the active site at the TS2 structure. The main interaction distances are depicted with black broken lines. Distances are given in Å.

The proton transfer from Asp166 to O2γATP is favored with respect to the protonation of O1γATP because, as indicated previously, along the movement of the γ-phosphoryl group towards Ser17 in the phosphoryl transfer step, the O2γATP-Mg2 distance increases and the negative charge on O2γATP becomes less stabilized (the Mg2-O2γATP distance increases from 2. 02 Å at $R_a$ to 2.21 Å at P1 and to 2.44 Å at TS2). A relevant change in the coordination sphere of the Mg2 ion along the catalytic mechanism has been recently observed in two crystallographic structures of PKA-$Mg_2$ADP-pSP20 complex showing partial or total phosphoryl transfer (structures with 4HPU and 4HPT PDB IDs, respectively).[18]

In contrast, the O1γATP atom which is somewhat more distant from Asp166 than O2γATP (the O1γATP- Oδ2Asp166 distance is 3.65 Å while the O2γATP- Oδ2Asp166 distance is 3.43 Å) is also more stabilized by its interaction with the Mg1 ion. That is, O1γATP has not such a basic character as O2γATP because O1γATP does not distance from Mg1 along the phosphoryl transfer. The Mg1-O1γATP distance only changes from 2.06 Å at $R_a$ to 2.12 Å at P1 and to 2.11 Å at TS2. Moreover, the conformation adopted by Lys168 is also crucial for the viability of the proton transfer step to O2γATP. As noted above from the values given in Table 3 and Figures 3A and 3B, at $R_a$ Lys168 is further away from O2γATP (3.41 Å) than at $R_b$ (2.85 Å) what contributes to enhance the basic character of O2γATP.

In this way we have demonstrated using a complete model of the solvated ternary complex PKA-$Mg_2$-ATP-Kemptide that the role of Asp166 as a general acid-base catalyst is viable in agreement with mutagenesis experiments. As indicated in the Introduction section, the important reduction in phosphorylation and in phosphopeptide release rate constants measured in the Asp149Asn mutant of PhK was explained by the incapability of Asn to ionize like Asp149.[51] The proton transfer from Ser17 of Kemptide to Asp166 (acting as a base catalyst) facilitates the phosphoryl transfer whereas the proton transfer from Asp166 (acting as an acid catalyst) to O2γATP regenerates the original protonation state of the enzyme. Anyway it has to be noted that Asp166 does not act as a conventional acid catalyst because its proton transfer begins after the corresponding transition state structure of the process. Moreover, it has also been suggested that the repulsion between the negatively charged Asp166 and the phosphopeptide product could facilitate the phosphopeptide dissociation and could also contribute in part to the rotation of the glycine-rich loop.[10] This is one of the conformational changes needed for the opening of the active site and the departure of the phosphorylated product and ADP.

**Conclusions**

In this paper the phosphorylation of Kemptide, an heptapeptide synthetic substrate of cAMP-dependent protein kinase A (PKA), has been studied by means of QM/MM calculations at the B3LYP/6-31+G(d)/CHARMM level with a complete solvated PKA-$Mg_2$ATP-Kemptide model. Single point energy calculations have been done at the higher MP2/cc-pVTZ/CHARMM level. The starting structures for this study were taken from a previous MD simulation of the PKA ternary Michaelis complex initiated from the 1CDK crystallographic X-ray structure, which presents a close active conformation with only residue Thr197 modified into a phospho-threonine. Due to the dependence of the energetics of the catalytic mechanism on the structure of the ternary PKA-$Mg_2$ATP-substrate complex and the substrate, it is important to analyze different systems.

The plausibility of the so-called concerted loose mechanism has been demonstrated for the Kemptide substrate in accordance with our previous study on the same system, but, in that case, only low level QM/MM calculations could be carried out, and a less efficient reaction coordinate was used. Our results are also in agreement with other studies using other structures of PKA and other ligands. However, our calculations demonstrate for the first time in a complete model of the ternary system the viability of the final step of the catalytic mechanism in which the protonation of the phosphokemptide product by Asp166 takes place. In this way, Asp166 would behave as a base catalyst by abstracting the HγSer17 of the Kemptide substrate what, in turn, enhances the nucleophilic character of the Ser17 side chain, thus facilitating the phosphoryl transfer. In a second step, Asp166 would also act as an acid catalyst by donating the proton just accepted from Ser17 to the O2γATP atom of the phosphoryl group. The charge repulsion between the negatively charged protonated phosphokemptide and the carboxylate group of Asp166 could facilitate product release in agreement with mutagenesis experiments. The precise location and orientation of the catalytic triad Lys168-Thr201-Asp166 have been shown to make a relevant contribution to the stabilization of the phosphoryl transfer (first step) and the proton transfer (second step) of the catalytic mechanism by modulating electrostatic and hydrogen bond interactions. Further studies on this catalytic mechanism with comparison purposes using other substrates and new X-ray structures recently deposited in the PDB, are being developed in our laboratory.

**Acknowledgments**

This work was supported by the “Ministerio de Economía y Competitividad” through Project CTQ2011-24292. We acknowledge recognition of our group by the “Generalitat de Catalunya” through Project 2014SGR94. Use of computational facilities at the “Consorci de Serveis

Científics i Acadèmics de Catalunya" (CSUC) is also gratefully acknowledged. Ayax Pérez-Gallegos acknowledges "Consejo Nacional de Ciencia y Tecnología" (CONACYT) Supporting Grant 213582.

**References**

1. G. Manning, D. B. Whyte, R. Martinez, T. Hunter and S. Sudarsanam, *Science*, 2002, **298**, 1912.
2. P. Cohen and D. R. Alessi, *ACS Chem. Biol.*, 2013, **8**, 96.
3. J. A. Adams, *Chem. Rev.*, 2001, **101**, 2271.
4. D. A. Walsh, J. P. Perkins and E. G. Krebs, *J. Biol. Chem.*, 1968, **243**, 3763.
5. D. Knighton, J. Zheng, L. Ten Eyck, V. Ashford, N. Xuong, S. Taylor and J. Sowadski, *Science*, 1991, **253**, 407.
6. D. Knighton, J. Zheng, L. Ten Eyck, N. Xuong, S. Taylor and J. Sowadski, *Science*, 1991, **253**, 414.
7. S. S. Taylor, J. Bubis, J. Toner-Webb, L. D. Saraswat, E. A. First, J. A. Buechler, D. R. Knighton and J. Sowadski, *FASEB J.*, 1988, **2**, 2677.
8. S. S. Taylor, D. R. Knighton, J. Zheng, L. F. Ten Eyck and J. M. Sowadski, *Annu. Rev. Cell Biol.*, 1992, **8**, 429.
9. D. A. Johnson, P. Akamine, E. Radzio-Andzelm, Madhusudan and S. S. Taylor, *Chem. Rev.*, 2001, **101**, 2243.
10. Madhusudan, E. A. Trafny, N.-H. Xuong, J. A. Adams, L. F. T. Eyck, S. S. Taylor and J. M. Sowadski, *Protein Sci.*, 1994, **3**, 176.
11. B. E. Kemp, D. J. Graves, E. Benjamini and E. G. Krebs, *J. Biol. Chem.*, 1977, **252**, 4888.
12. R. Qamar, M. Y. Yoon and P. F. Cook, *Biochemistry*, 1992, **31**, 9986.
13. J. A. Adams and S. S. Taylor, *Biochemistry*, 1992, **31**, 8516.
14. B. D. Grant and J. A. Adams, *Biochemistry*, 1996, **35**, 2022.
15. C. Li, N. Ma, Y. Wang, Y. Wang and G. Chen, *J. Phys. Chem. B*, 2014, **118**, 1273.
16. P. C. Sims, I. S. Moody, Y. Choi, C. Dong, M. Iftikhar, B. L. Corso, O. T. Gul, P. G. Collins and G. A. Weiss, *J. Am. Chem. Soc.*, 2013, **135**, 7861.
17. S. S. Taylor, P. Zhang, J. M. Steichen, M. M. Keshwani and A. P. Kornev, *Biochim. Biophys. Acta*, 2013, **1834**, 1271.
18. A. C. Bastidas, M. S. Deal, J. M. Steichen, Y. Guo, J. Wu and S. S. Taylor, *J. Am. Chem. Soc.*, 2013, **135**, 4788.
19. O. Gerlits, M. J. Waltman, S. Taylor, P. Langan and A. Kovalevsky, *Biochemistry*, 2013, **52**, 3721.
20. M. Montenegro, L. Masgrau, À. González-Lafont, J. M. Lluch and M. Garcia-Viloca, *Biophys. Chem.*, 2012, **161**, 17.
21. D. M. Jacobsen, Z.-Q. Bao, P. O'Brien, C. L. Brooks and M. A. Young, *J. Am. Chem. Soc.*, 2012, **134**, 15357.
22. B. R. Prasad, N. V. Plotnikov and A. Warshel, *J. Phys. Chem. B*, 2013, **117**, 153.
23. N. V. Plotnikov, B. R. Prasad, S. Chakrabarty, Z. T. Chu and A. Warshel, *J. Phys. Chem. B*, 2013, **117**, 12807.
24. J. K. Lassila, J. G. Zalatan and D. Herschlag, *Annu. Rev. Biochem.*, 2011, **80**, 669.
25. Y. Jin, M. J. Cliff, N. J. Baxter, H. R. W. Dannatt, A. M. Hounslow, M. W. Bowler, G. M. Blackburn and J. P. Waltho, *Angew. Chem. Int. Ed.*, 2012, **51**, 12242.
26. O. Gerlits, A. Das, M. M. Keshwani, S. Taylor, M. J. Waltman, P. Langan, W. T. Heller and A. Kovalevsky, *Biochemistry*, 2014, **53**, 3179.
27. L. R. Masterson, L. Shi, E. Metcalfe, J. Gao, S. S. Taylor and G. Veglia, *Proc. Natl. Acad. Sci. USA*, 2011, **108**, 6969.
28. L. R. Masterson, A. Cembran, L. Shi and G. Veglia, *Adv. Protein Chem. Struct. Biol.*, 2012, **87**, 363.
29. I. V. Khavrutskii, B. Grant, S. S. Taylor and J. A. McCammon, *Biochemistry*, 2009, **48**, 11532.
30. M. Valiev, R. Kawai, J. A. Adams and J. H. Weare, *J. Am. Chem. Soc.*, 2003, **125**, 9926.
31. N. Díaz and M. J. Field, *J. Am. Chem. Soc.*, 2004, **126**, 529.
32. Y. Cheng, Y. Zhang and J. A. McCammon, *J. Am. Chem. Soc.*, 2005, **127**, 1553.
33. Y. Cheng, Y. Zhang and J. A. McCammon, *Protein Sci.*, 2006, **15**, 672.
34. M. Valiev, J. Yang, J. A. Adams, S. S. Taylor and J. H. Weare, *J. Phys. Chem. B*, 2007, **111**, 13455.

35. M. Montenegro, M. Garcia-Viloca, À. González-Lafont and J. Lluch, *J. Comput. Aided Mol. Des.*, 2007, **21**, 603.
36. M. Montenegro, M. Garcia-Viloca, J. M. Lluch and A. Gonzalez-Lafont, *Phys. Chem. Chem. Phys.*, 2011, **13**, 530.
37. G. K. Smith, Z. Ke, H. Guo and A. C. Hengge, *J. Phys. Chem. B*, 2011, **115**, 13713.
38. A. Pérez-Gallegos, M. Garcia-Viloca, À. González-Lafont and J. Lluch, *J. Comput. Aided Mol. Des.*, 2014, **28,** 1077.
39. S. S. Taylor, J. Yang, J. Wu, N. M. Haste, E. Radzio-Andzelm and G. Anand, *Biochim. Biophys. Acta*, 2004, **1697**, 259.
40. L. R. Masterson, C. Cheng, T. Yu, M. Tonelli, A. Kornev, S. S. Taylor and G. Veglia, *Nat. Chem. Biol.*, 2010, **6**, 821.
41. A. Cembran, L. R. Masterson, C. L. McClendon, S. S. Taylor, J. Gao and G. Veglia, *Biochemistry*, 2012, **51**, 10186.
42. J. Yang, L. F. Ten Eyck, N.-H. Xuong and S. S. Taylor, *J. Mol. Biol.*, 2004, **336**, 473.
43. A. Y. Kovalevsky, H. Johnson, B. L. Hanson, M. J. Waltman, S. Z. Fisher, S. Taylor and P. Langan, *Acta Crystallogr. D Biol. Crystallogr.*, 2012, **68**, 854.
44. Madhusudan, P. Akamine, N.-H. Xuong and S. S. Taylor, *Nat. Struct. Mol. Biol.*, 2002, **9**, 273.
45. J. C. Hart, D. W. Sheppard, I. H. Hillier and N. A. Burton, *Chem. Commun.*, 1999, 79.
46. D. W. Sheppard, N. A. Burton and I. H. Hillier, *J. Mol. Struct. (THEOCHEM)*, 2000, **506**, 35.
47. M. C. Hutter and V. Helms, *Int. J. Quantum Chem.*, 2003, **95**, 479.
48. J. Zheng, E. A. Trafny, D. R. Knighton, N. Xuong, S. S. Taylor, L. F. Ten Eyck and J. M. Sowadski, *Acta Crystallographica Section D*, 1993, **49**, 362.
49. D. Bossemeyer, R. Engh, V. Kinzel, H. Ponstingl and R. Huber, *EMBO J.*, 1993, **12**, 849.
50. C. S. Gibbs and M. J. Zoller, *J. Biol. Chem.*, 1991, **266**, 8923.
51. V. T. Skamnaki, D. J. Owen, M. E. M. Noble, E. D. Lowe, G. Lowe, N. G. Oikonomakos and L. N. Johnson, *Biochemistry*, 1999, **38**, 14718.
52. J. Zhou and J. A. Adams, *Biochemistry*, 1997, **36**, 2977.
53. J. Zhou and J. A. Adams, *Biochemistry*, 1997, **36**, 15733.
54. W. Humphrey, A. Dalke and K. Schulten, *J. Mol. Graph.*, 1996, **14**, 33.
55. P. Sherwood, A. H. de Vries, M. F. Guest, G. Schreckenbach, C. R. A. Catlow, S. A. French, A. A. Sokol, S. T. Bromley, W. Thiel, A. J. Turner, S. Billeter, F. Terstegen, S. Thiel, J. Kendrick, S. C. Rogers, J. Casci, M. Watson, F. King, E. Karlsen, M. Sjøvoll, A. Fahmi, A. Schäfer and C. Lennartz, *J. Mol. Struct. (THEOCHEM)*, 2003, **632**, 1.
56. R. Ahlrichs, M. Bär, M. Häser, H. Horn and C. Kölmel, *Chem. Phys. Lett.*, 1989, **162**, 165.
57. A. D. Becke, *J. Chem. Phys.*, 1993, **98**, 5648.
58. P. J. Stephens, F. J. Devlin, C. F. Chabalowski and M. J. Frisch, *J. Phys. Chem.*, 1994, **98**, 11623.
59. C. Lee, W. Yang and R. G. Parr, *Phys. Rev. B*, 1988, **37**, 785.
60. M. M. Francl, W. J. Pietro, W. J. Hehre, J. S. Binkley, M. S. Gordon, D. J. DeFrees and J. A. Pople, *J. Chem. Phys.*, 1982, **77**, 3654.
61. T. Clark, J. Chandrasekhar, G. W. Spitznagel and P. V. R. Schleyer, *J. Comput. Chem.*, 1983, **4**, 294.
62. W. Smith and T. R. Forester, *J. Mol. Graph.*, 1996, **14**, 136.
63. A. D. MacKerell, D. Bashford, M. Bellott, R. L. Dunbrack, J. D. Evanseck, M. J. Field, S. Fischer, J. Gao, H. Guo, S. Ha, D. Joseph-McCarthy, L. Kuchnir, K. Kuczera, F. T. K. Lau, C. Mattos, S. Michnick, T. Ngo, D. T. Nguyen, B. Prodhom, W. E. Reiher, B. Roux, M. Schlenkrich, J. C. Smith, R. Stote, J. Straub, M. Watanabe, J. Wiórkiewicz-Kuczera, D. Yin and M. Karplus, *J. Phys. Chem. B*, 1998, **102**, 3586.
64. A. D. MacKerell, M. Feig and C. L. Brooks, *J. Am. Chem. Soc.*, 2003, **126**, 698.
65. M. Montenegro, M. Garcia-Viloca, À. González-Lafont and J. Lluch, *Theor. Chem. Acc.*, 2009, **124**, 197.
66. A. H. de Vries, P. Sherwood, S. J. Collins, A. M. Rigby, M. Rigutto and G. J. Kramer, *J. Phys. Chem. B*, 1999, **103**, 6133.
67. H. M. Senn and W. Thiel, *Angew. Chem. Int. Ed.*, 2009, **48**, 1198.
68. D. Liu and J. Nocedal, *Math. Prog.*, 1989, **45**, 503.
69. A. J. Turner, V. Moliner and I. H. Williams, *Phys. Chem. Chem. Phys.*, 1999, **1**, 1323.
70. S. R. Billeter, A. J. Turner and W. Thiel, *Phys. Chem. Chem. Phys.*, 2000, **2**, 2177.
71. J. Baker, *J. Comput. Chem.*, 1986, **7**, 385.

72. A. E. Reed, R. B. Weinstock and F. Weinhold, *J. Chem. Phys.*, 1985, **83**, 735.
73. M. Head-Gordon, J. A. Pople and M. J. Frisch, *Chem. Phys. Lett.*, 1988, **153**, 503.
74. D. E. Woon and T. H. Dunning, *J. Chem. Phys.*, 1993, **98**, 1358.
75. J. Lew, S. S. Taylor and J. A. Adams, *Biochemistry*, 1997, **36**, 6717.